Electronic Supplementary Material (ESI) for Soft Matter.

Supporting Information

Characterisation of hydration and nanophase-separation during the temperature response in hydrophobic/hydrophilic elastin-like polypeptide (ELP) diblock copolymers

Katharina Widder,*[a] Sarah MacEwan,[b] Elisabeth Garanger,[c]
Vanesa Núñez,[a] Sébastien Lecommandoux,[c] Ashutosh Chilkoti[b]
and Dariush Hinderberger[a]

[a] *Institut für Chemie, Martin-Luther-Universität Halle-Wittenberg, Von-Danckelmann-Platz 4, 06118 Halle (Saale), Germany. E-mail: dariush.hinderberger@chemie.uni-halle.de*

[b] *Department of Biomedical Engineering, Duke University, 136 Hudson Hall, Campus Box 90281 Durham, North Carolina 27708, United States.*

[c] *Laboratoire de Chimie des Polymères Organiques, CNRS UMR 5629, Université de Bordeaux, Bordeaux-INP, Pessac 33607 Cedex, France.*

1 Diblock ELP

The investigated ELPs were composed of the following amino acid sequences:

1. ELP 40-60: MGCGWPG-(VGVPG)$_{40}$-(AGVPGGGVPG)$_{30}$-PGGS
2. ELP 80-60: MGCGWPG-(VGVPG)$_{80}$-(AGVPGGGVPG)$_{30}$-PGGS
3. ELP 120-60: MGCGWPG-(VGVPG)$_{120}$-(AGVPGGGVPG)$_{30}$-PGGS
4. ELP 200-60: MGCGWPG-(VGVPG)$_{200}$-(AGVPGGGVPG)$_{30}$-PGGS
5. ELP 200-30: GCGWPG-(VGVPG)$_{200}$-(AGVPGGGVPG)$_{15}$-PGGS
6. ELP 200-S30: GCGWPG-(VGVPG)$_{200}$-(SGVPG)$_{30}$-PGGS.

Diblock ELPs 200-30 and 200-S30 were cloned and produced in *E. coli* and fully characterized following previously established procedures.[1]

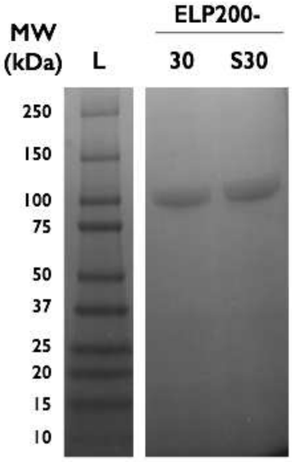

Figure SI 1: SDS-PAGE of diblock ELPs 200-30 (94.0 kDa) and 200-S30 (94.7 kDa)

Table SI 1: Characteristics of diblock ELPs 200-30 and 200-S30

ELP	MW in kDa	f	$T_{t/UV-Vis}$ in °C ($c = 25\,\mu$M)
200-30	94.0	0.12	24
200-S30	94.7	0.13	25

Equations of the exponential regression of the transition temperatures in Fig. 2 (main text):

$$T_t(f) = 19.71\,^\circ\text{C} + 1.44\,^\circ\text{C} \cdot \exp(4.53\,\frac{1}{^\circ\text{C}} \cdot f) \tag{1}$$

$$T_t(f) = 22.90\,^\circ\text{C} + 0.90\,^\circ\text{C} \cdot \exp(5.44\,\frac{1}{^\circ\text{C}} \cdot f). \tag{2}$$

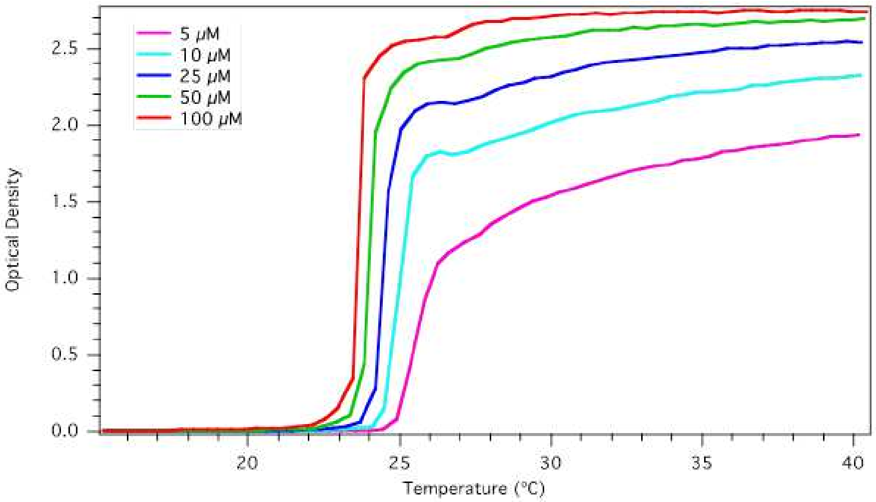

Figure SI 2: UV-Vis spectroscopy of diblock ELP 200-30 at different concentrations (5, 10, 25, 50 and 100 μM)

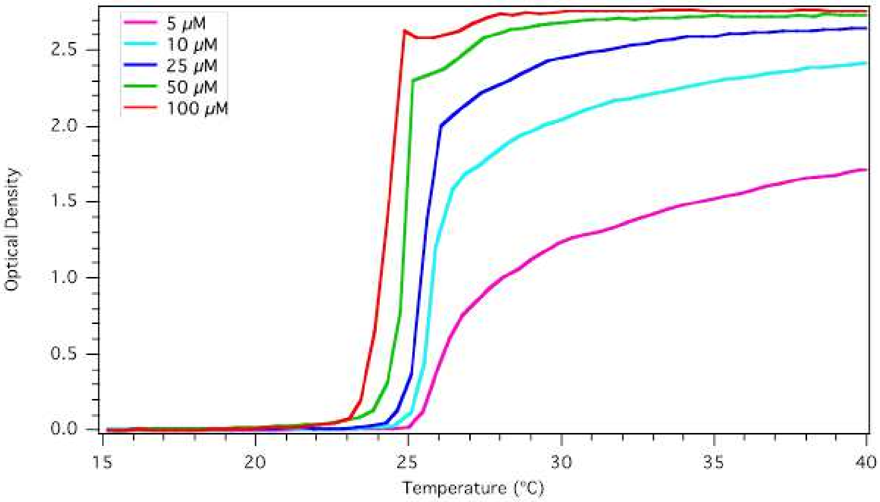

Figure SI 3: UV-Vis spectroscopy of diblock ELP 200-S30 at different concentrations (5, 10, 25, 50 and 100 μM)

2 Detected EPR spectra

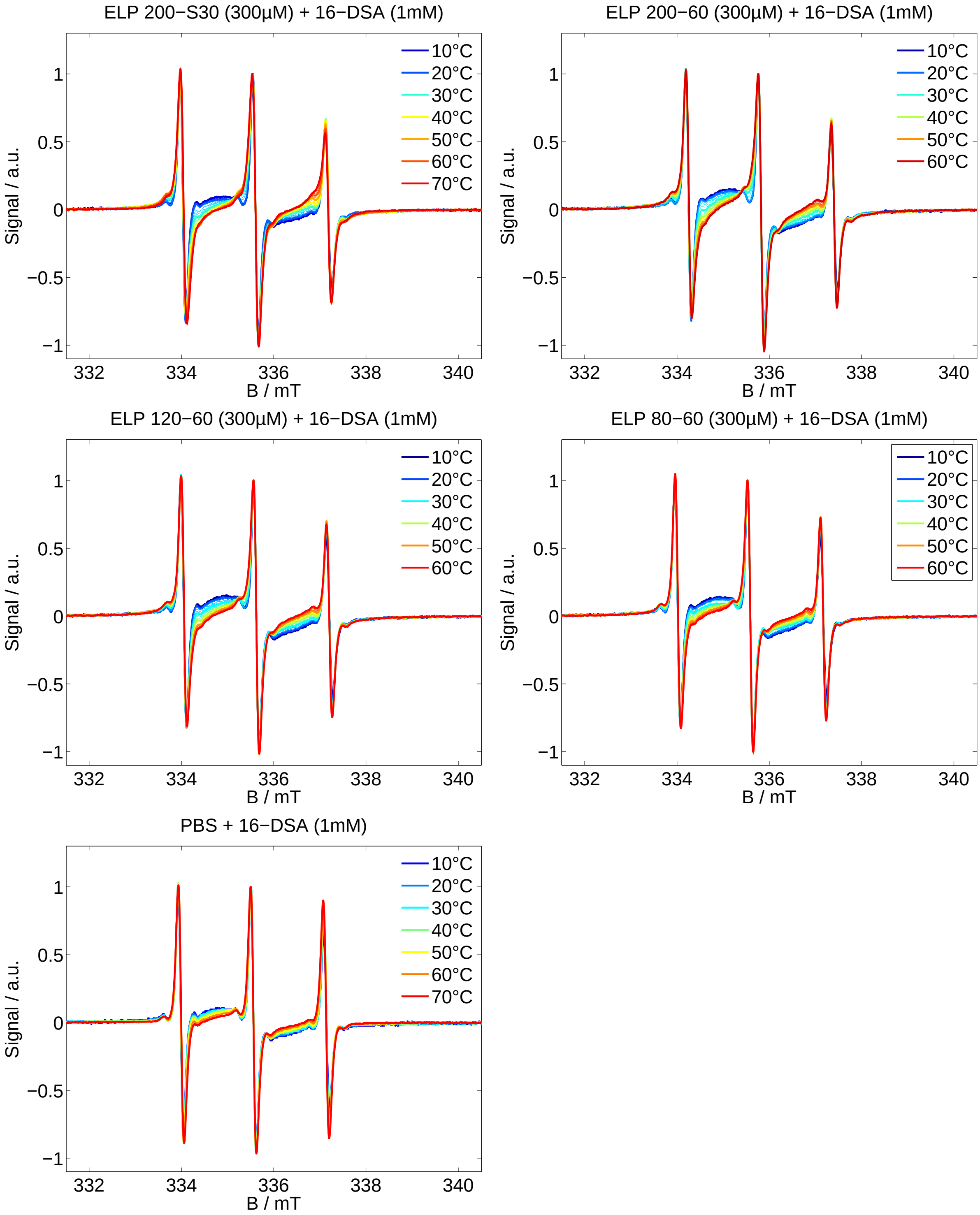

Figure SI 4: CW EPR spectra of the polymers with spin probe 16-DSA, which were not shown in the paper, and of 16-DSA in pure buffer (reference measurement)

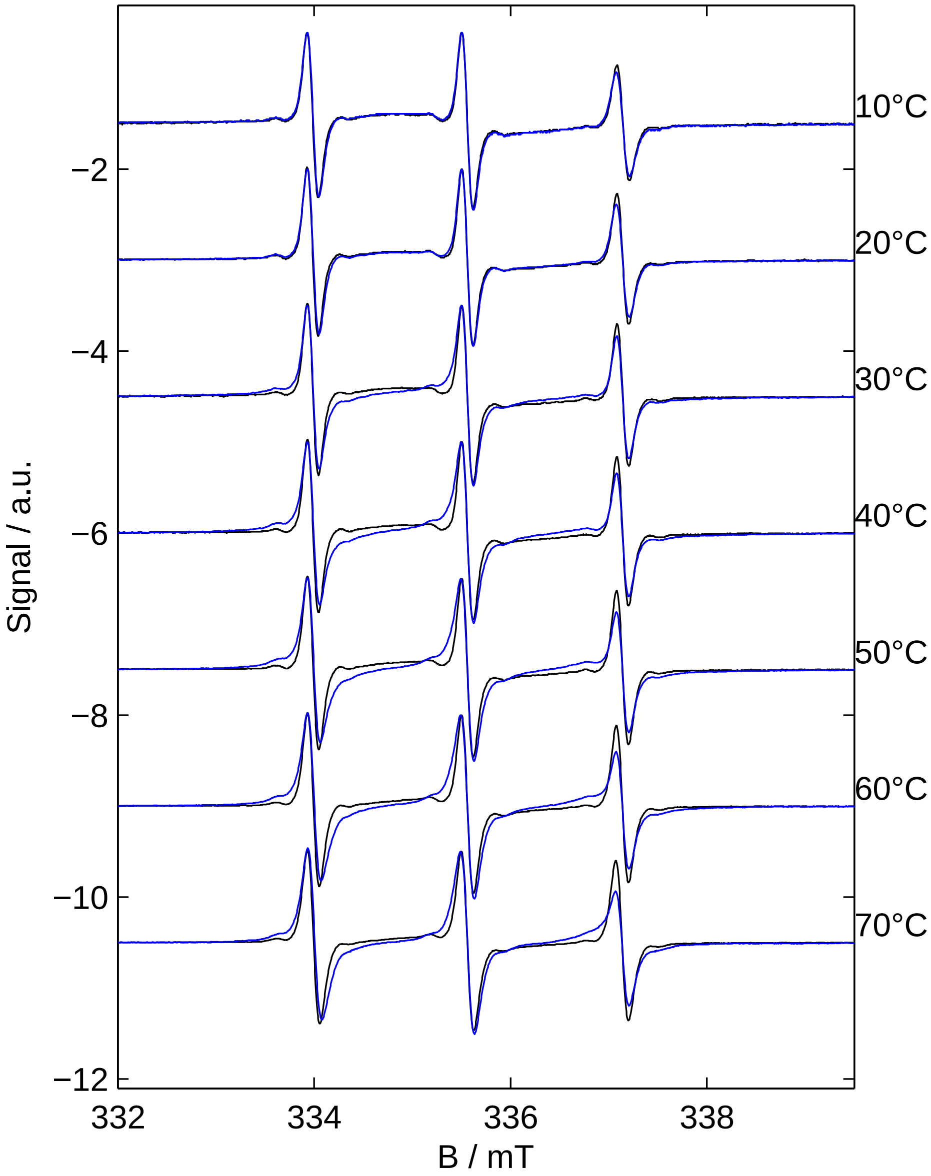

Figure SI 5: Superposition of EPR spectra of 16-DSA in pure buffer (black) and of ELP 200-30 (300 µM) with 16-DSA (1 mM) (blue) at temperatures between 10 and 70 °

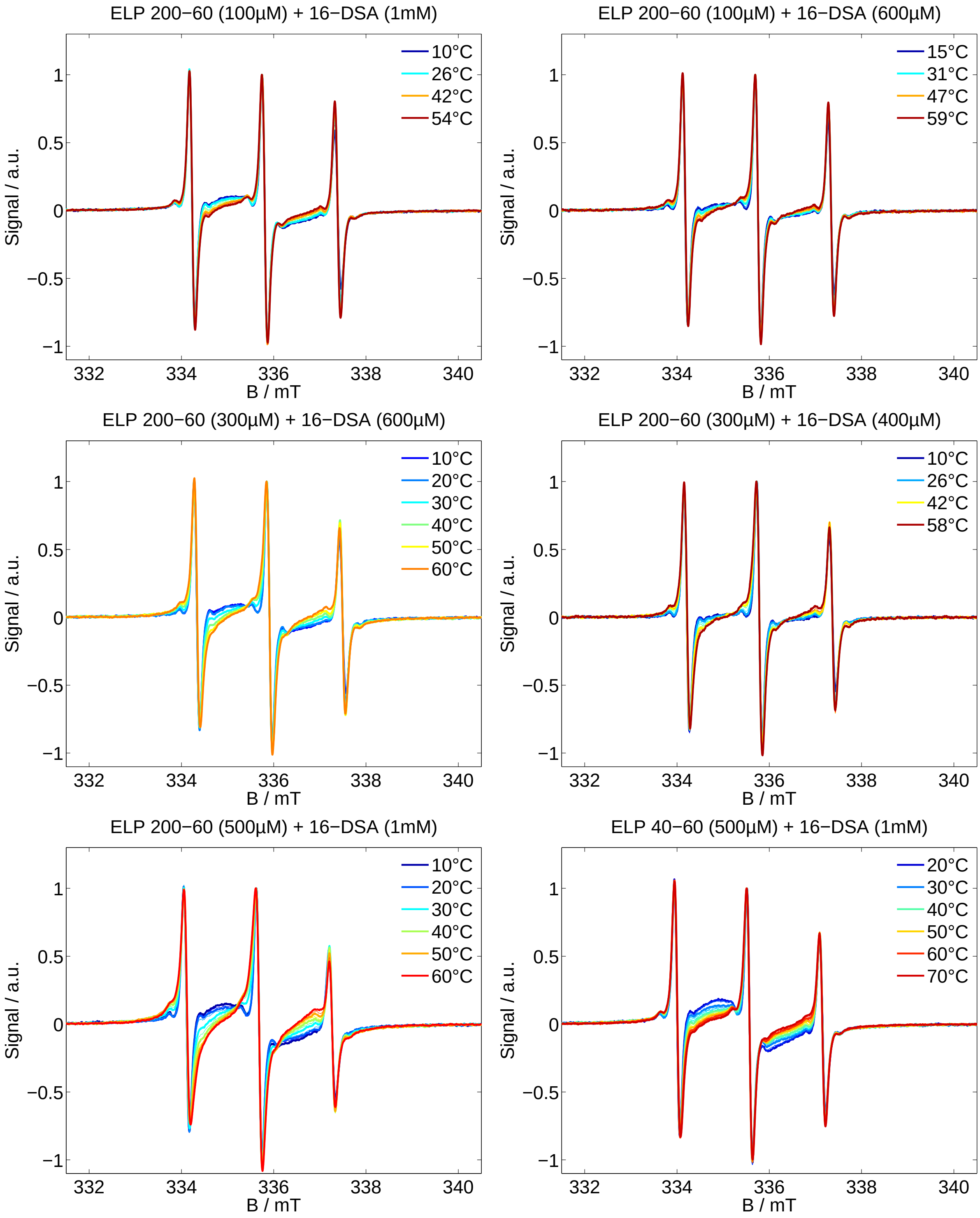

Figure SI 6: CW EPR spectra of different polymer concentrations with different concentrations of the spin probe 16-DSA

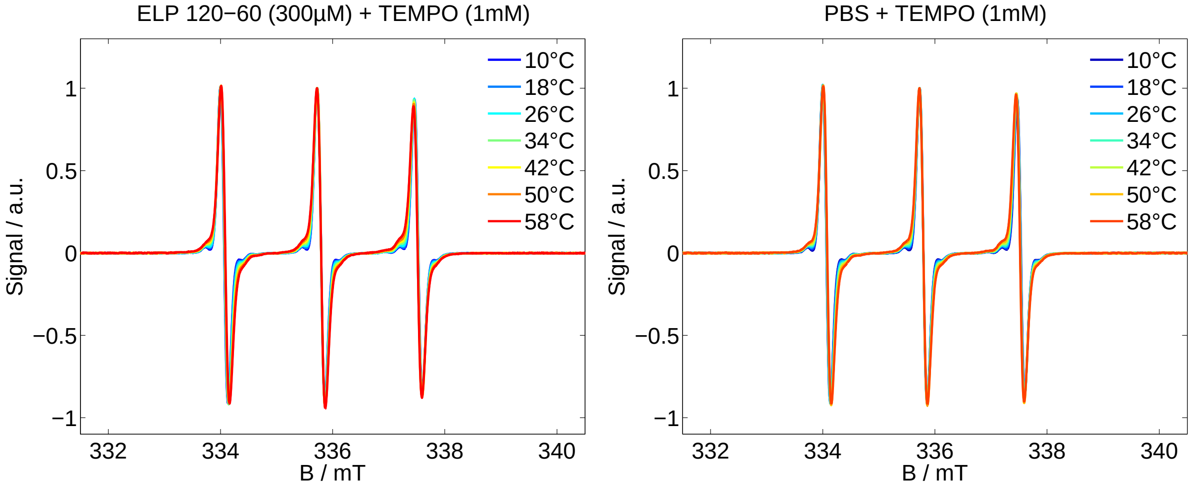

Figure SI 7: Test measurements with spin probe TEMPO: ELP 120-60 with TEMPO and reference measurement in PBS without polymer.

3 EPR Simulation

For the simulation of the EPR spectra home-written MATLAB routines for 3 component CW EPR spectra of nitroxide radicals were used by means of the software package EasySpin.[2] Parameters were obtained partly from literature and by adjusting them reasonable little by little until the difference between the measured and the simulated spectra is minimized.

Starting parameters for the values of the $\boldsymbol{g}$-tensor and for the hyperfine splitting tensor $\boldsymbol{A}$ were chosen considering Ge et al.[3] The values of A are used as a starting point. During the adjustment of all parameters, also A is adjusted to find the fit the hyperfine splitting of the measured EPR spectra. The same applies for g. The values of Ge et al. are used as a starting point especially for g_{yy} and g_{zz}, since the X-Band EPR spectrum is most influenced by g_{xx}. With an Mn-standard (Magnettech, Berlin, Germany) with well-known values for the positions of its six peaks the error of our $g = \frac{1}{3}(g_{xx} + g_{yy} + g_{zz})$ can be estimated ($\approx$4e-4). With g_{yy} and g_{zz} and corrected g_{iso} from Ref. 3, g_{xx} was adjusted. But these g-values are only of a qualitative character and should be measured by a W-Band spectrometer.

In case of the hydrophilic spectral component, the values were $\boldsymbol{g} = [g_{xx}\, g_{yy}\, g_{zz}] = [2.0086\, 2.0063\, 2.0025]$ and $\boldsymbol{A} = [A_{xx}\, A_{yy}\, A_{zz}] = [18.38\, 16.70\, 97.96]\,\text{MHz}$. The values of $\boldsymbol{A}$ refer to a temperature of $10\,^{\circ}\text{C}$. A_{xx} and A_{yy} slightly decrease with increasing temperatures due to the decreasing polarisability of water. Taking into account that the difference of g_{xx} between polar and apolar regions is not higher than 0.0004,[4,5] on has in case of the hydrophobic spectral component: $\boldsymbol{g} = [g_{xx}\, g_{yy}\, g_{zz}] = [2.0089\, 2.0063\, 2.0025]$ and $\boldsymbol{A} = [A_{xx}\, A_{yy}\, A_{zz}] = [17.98\, 15.90\, 94.55]\,\text{MHz}$.

4 Simulated EPR spectra

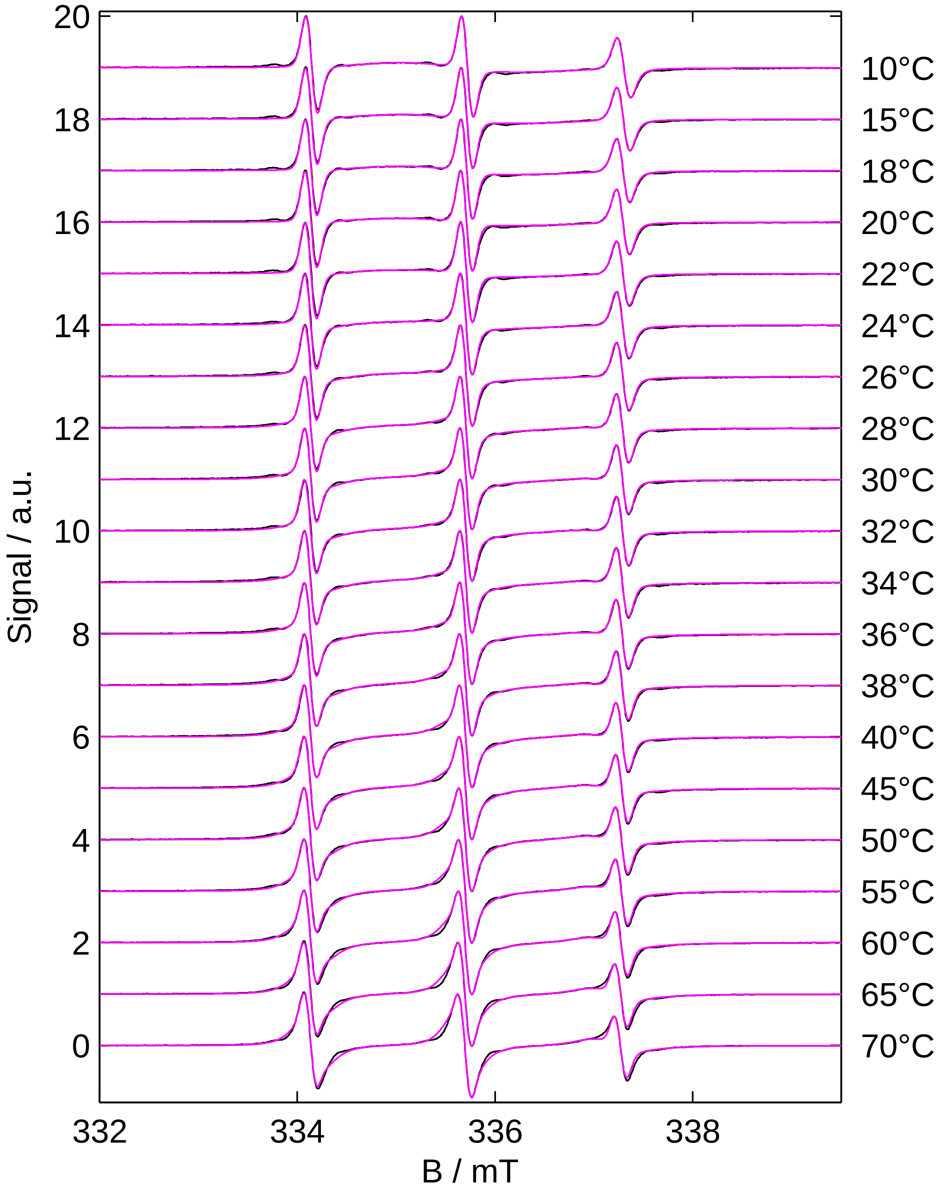

Figure SI 8: All EPR spectral simulations of ELP 200-S30 (300 µM) with 16-DSA (1 mM) at temperatures between 10 and 70 °C. Experimental data is shown in black, simulated data in magenta.

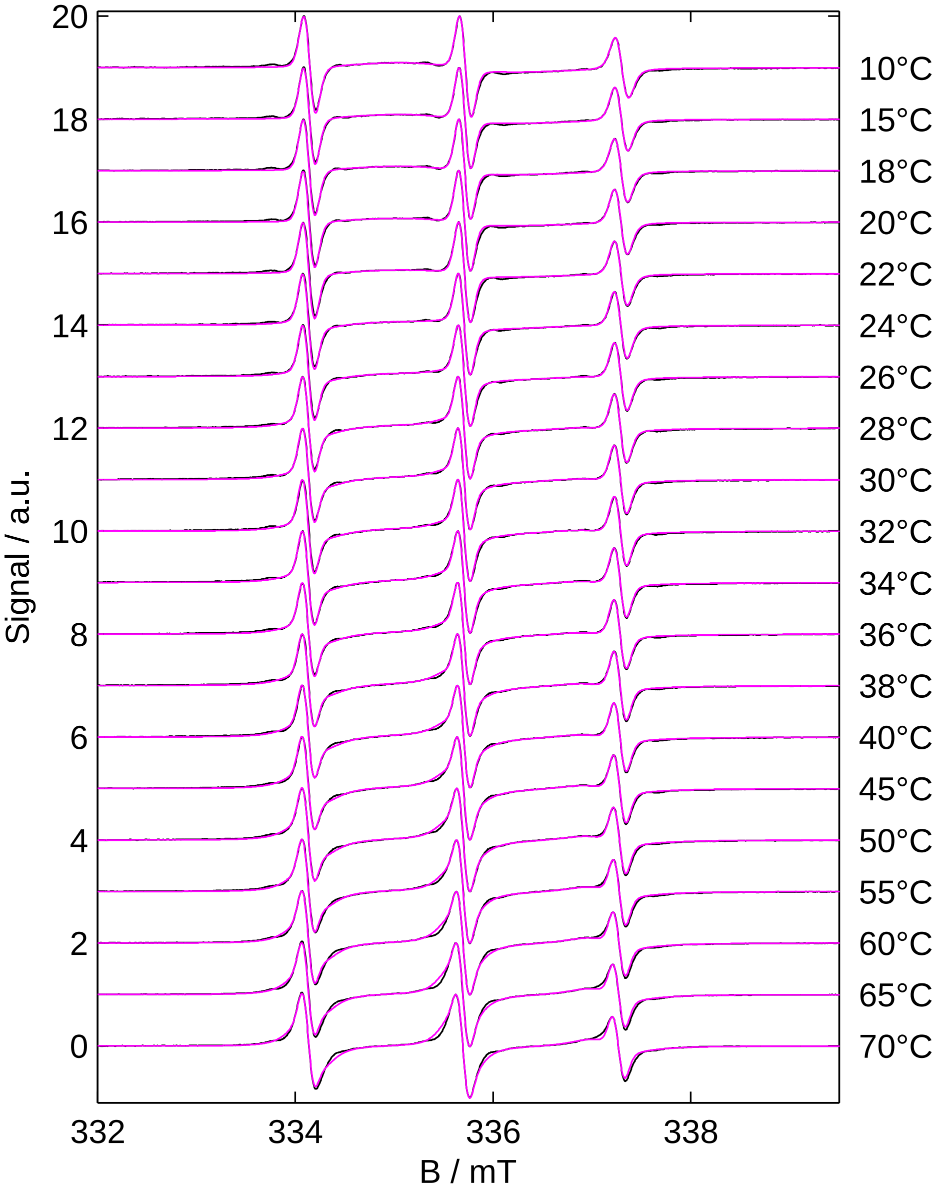

Figure SI 9: All EPR spectral simulations of ELP 200-30 (300 µM) with 16-DSA (1 mM) at temperatures between 10 and 70 °C. Experimental data is shown in black, simulated data in magenta.

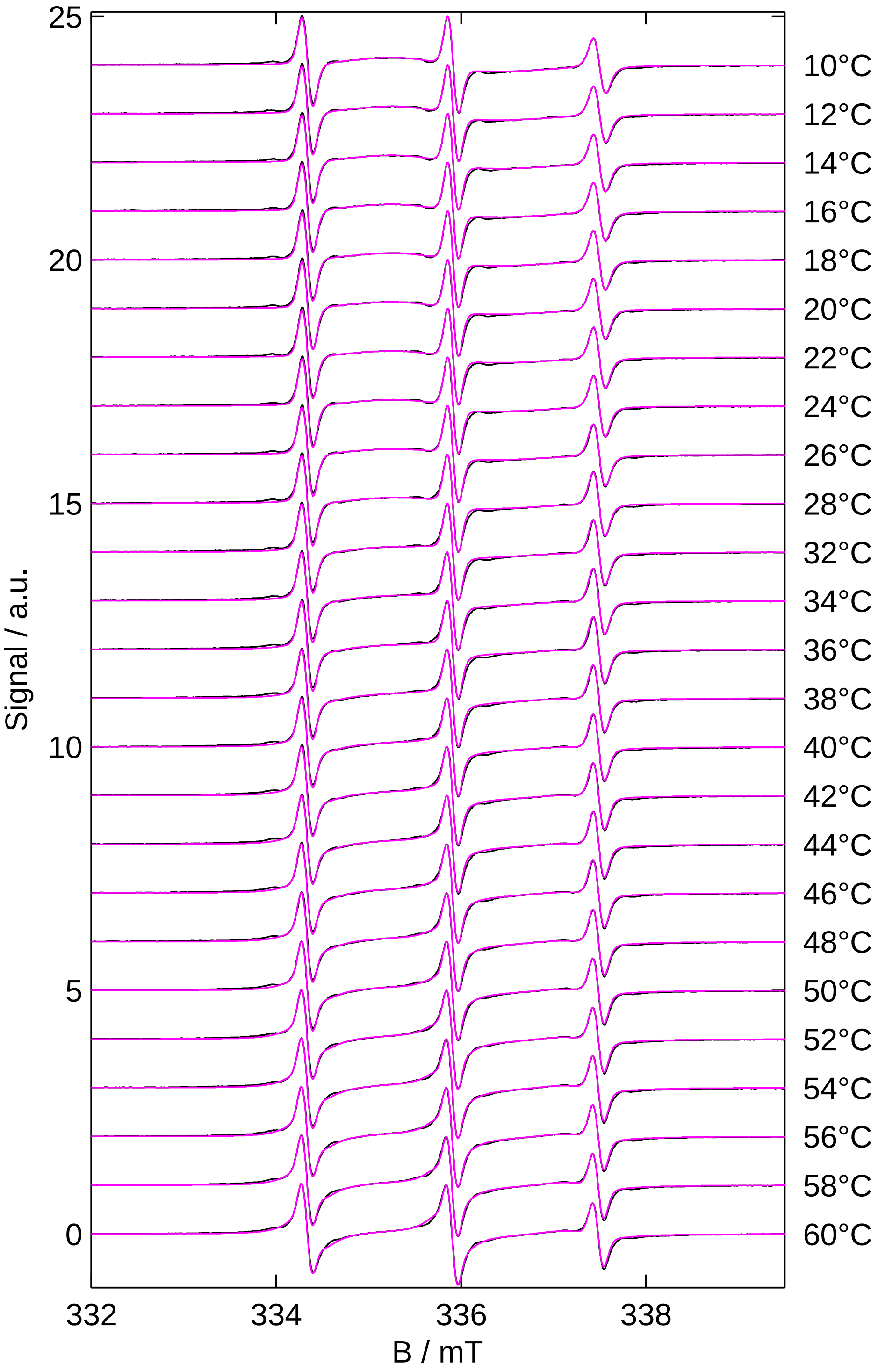

Figure SI 10: All EPR spectral simulations of ELP 200-60 (300 µM) with 16-DSA (1 mM) at temperatures between 10 and 60 °C. Experimental data is shown in black, simulated data in magenta.

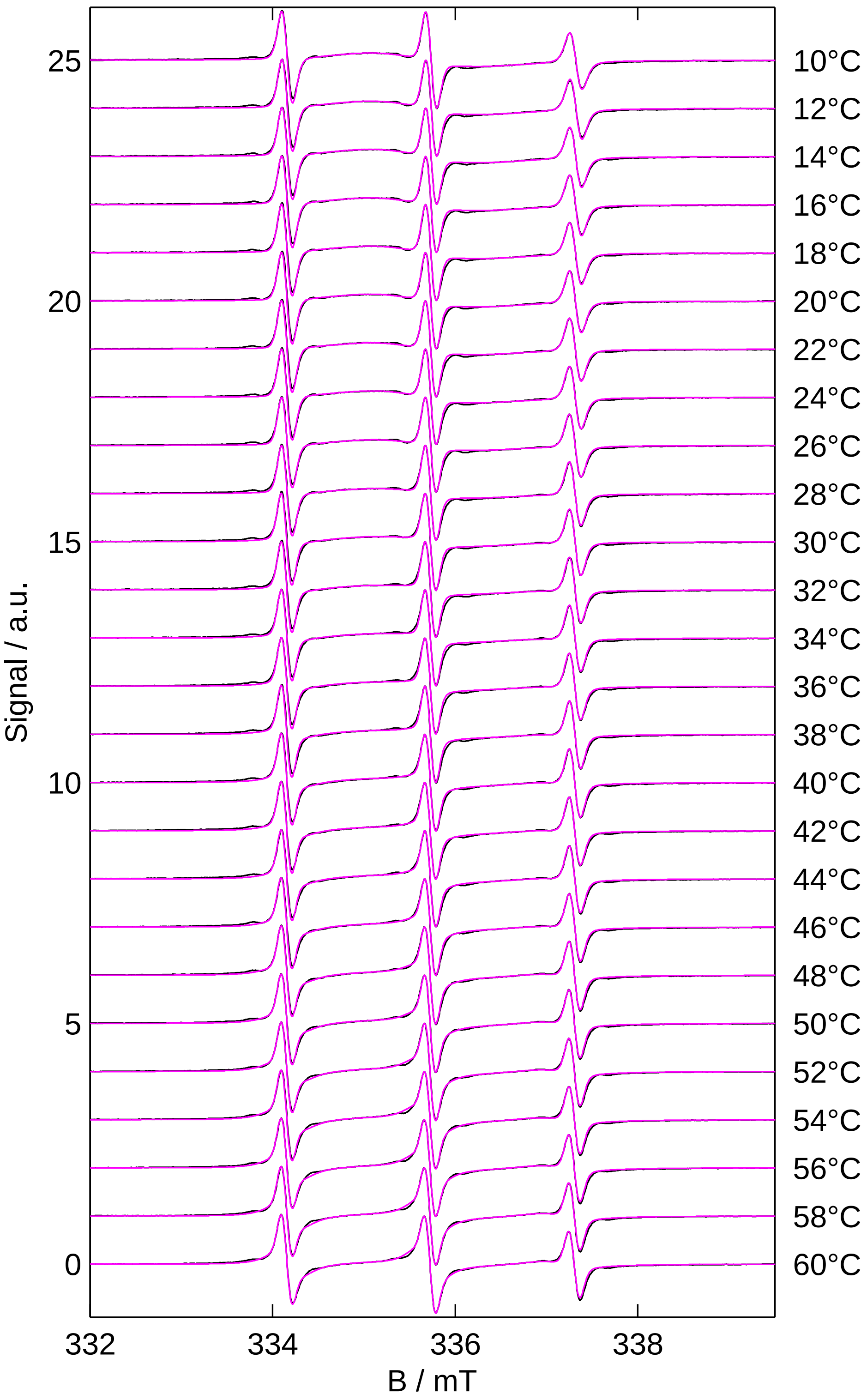

Figure SI 11: All EPR spectral simulations of ELP 120-60 (300 µM) with 16-DSA (1 mM) at temperatures between 10 and 60 °C. Experimental data is shown in black, simulated data in magenta.

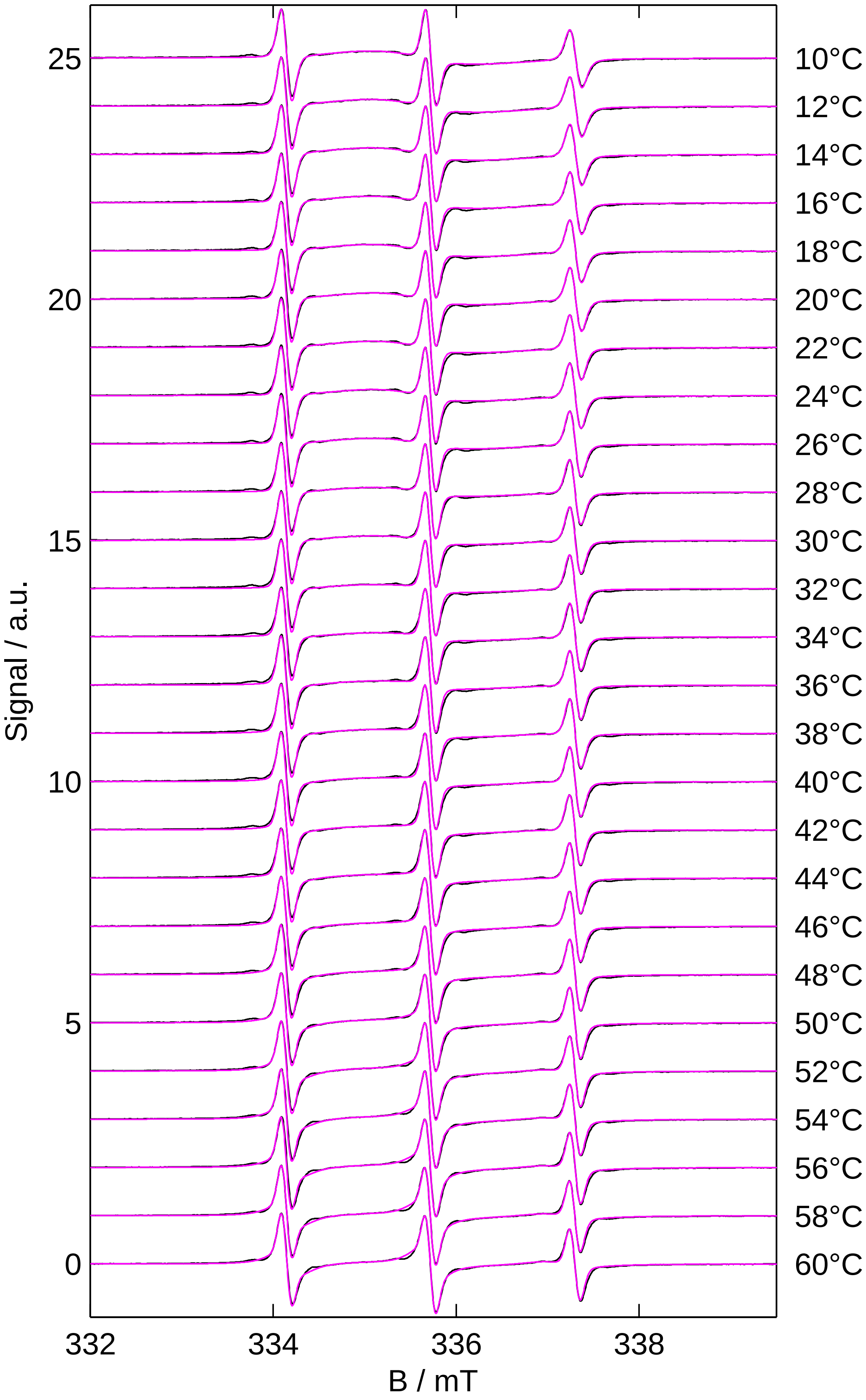

Figure SI 12: All EPR spectral simulations of ELP 80-60 (300 µM) with 16-DSA (1 mM) at temperatures between 10 and 60 °C. Experimental data is shown in black, simulated data in magenta.

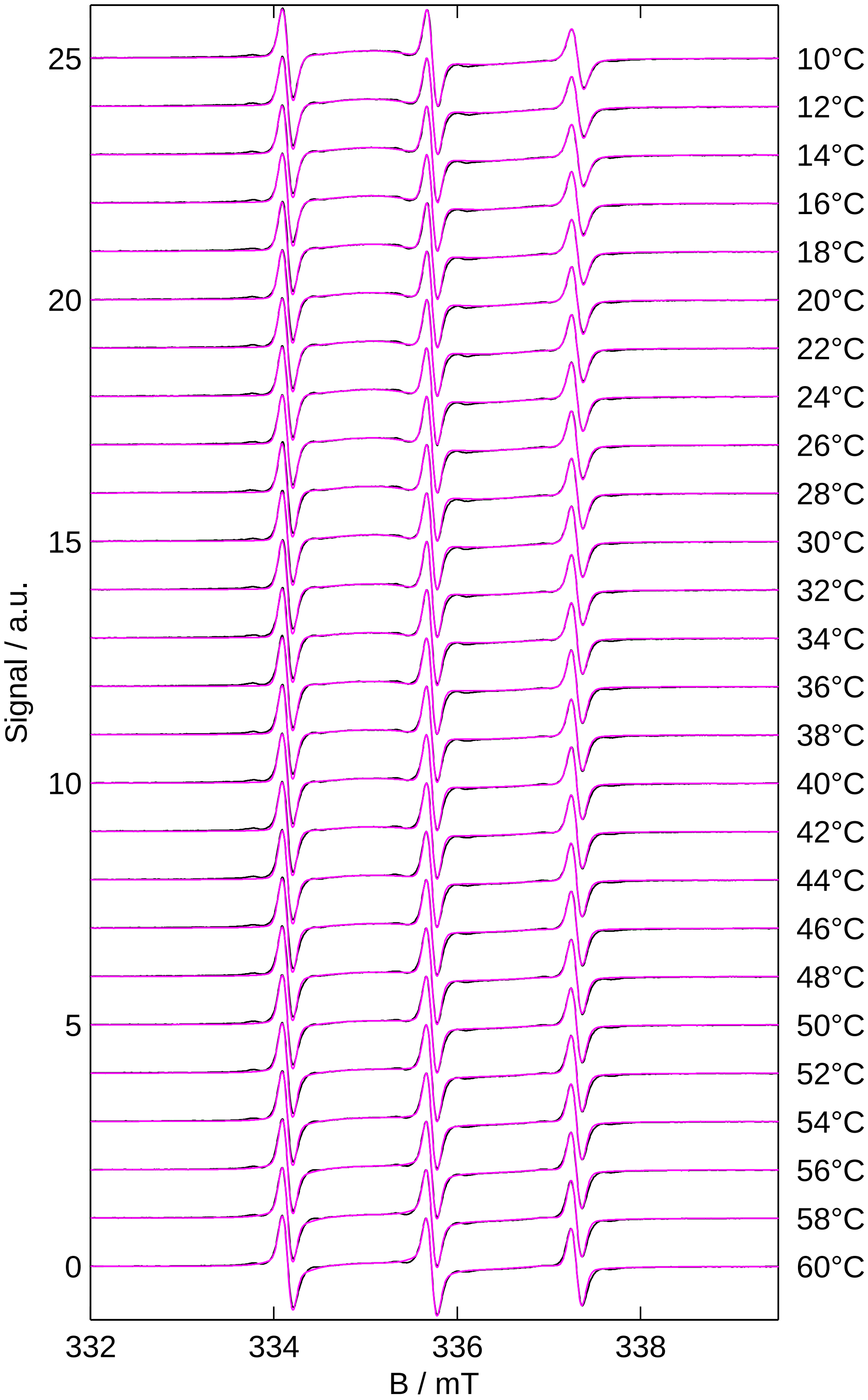

Figure SI 13: All EPR spectral simulations of ELP 40-60 (300 µM) with 16-DSA (1 mM) at temperatures between 10 and 60 °C. Experimental data is shown in black, simulated data in magenta.

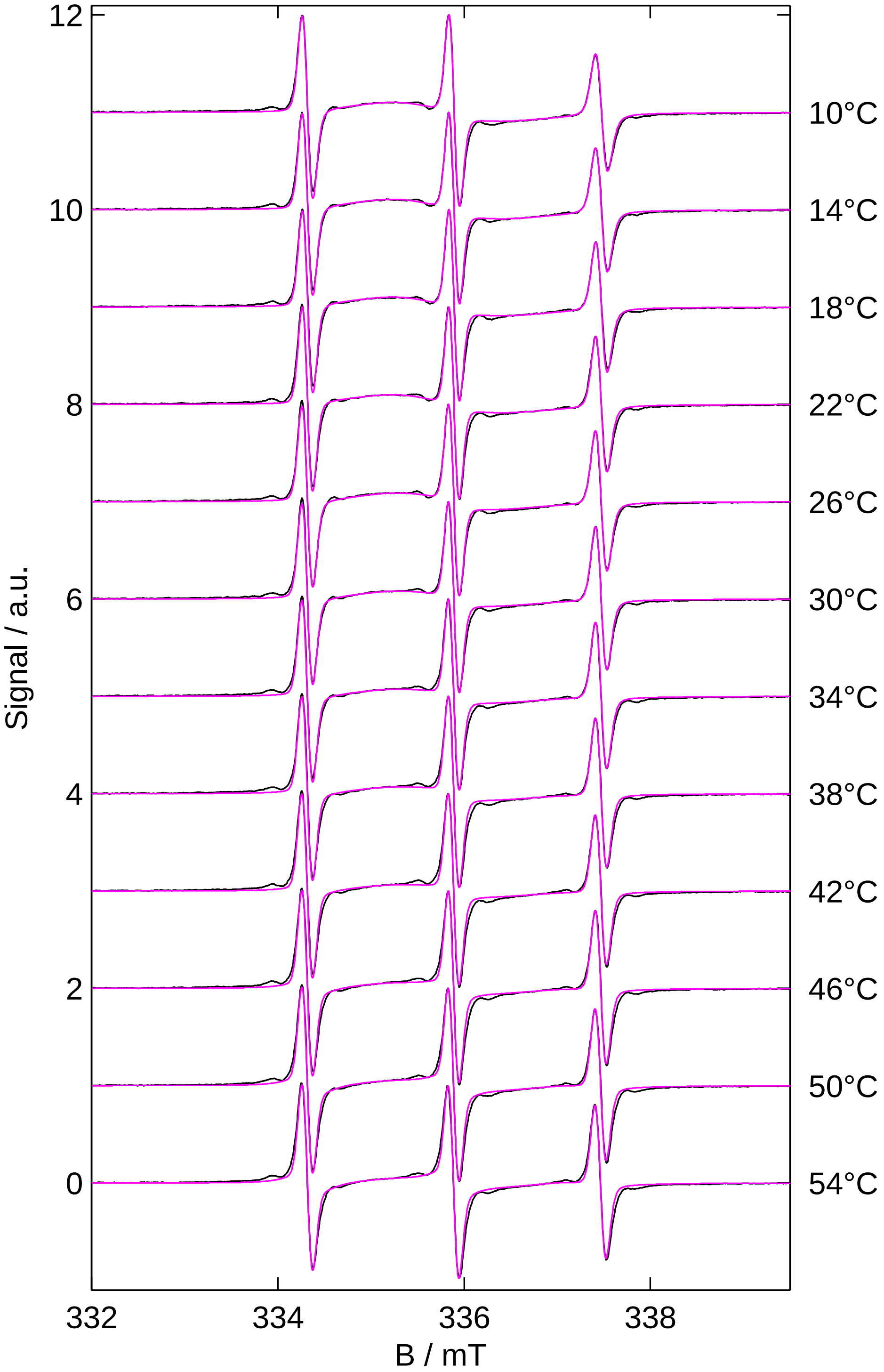

Figure SI 14: All EPR spectral simulations of ELP 200-60 (100 µM) with 16-DSA (1 mM) at temperatures between 10 and 54 °C. Experimental data is shown in black, simulated data in magenta.

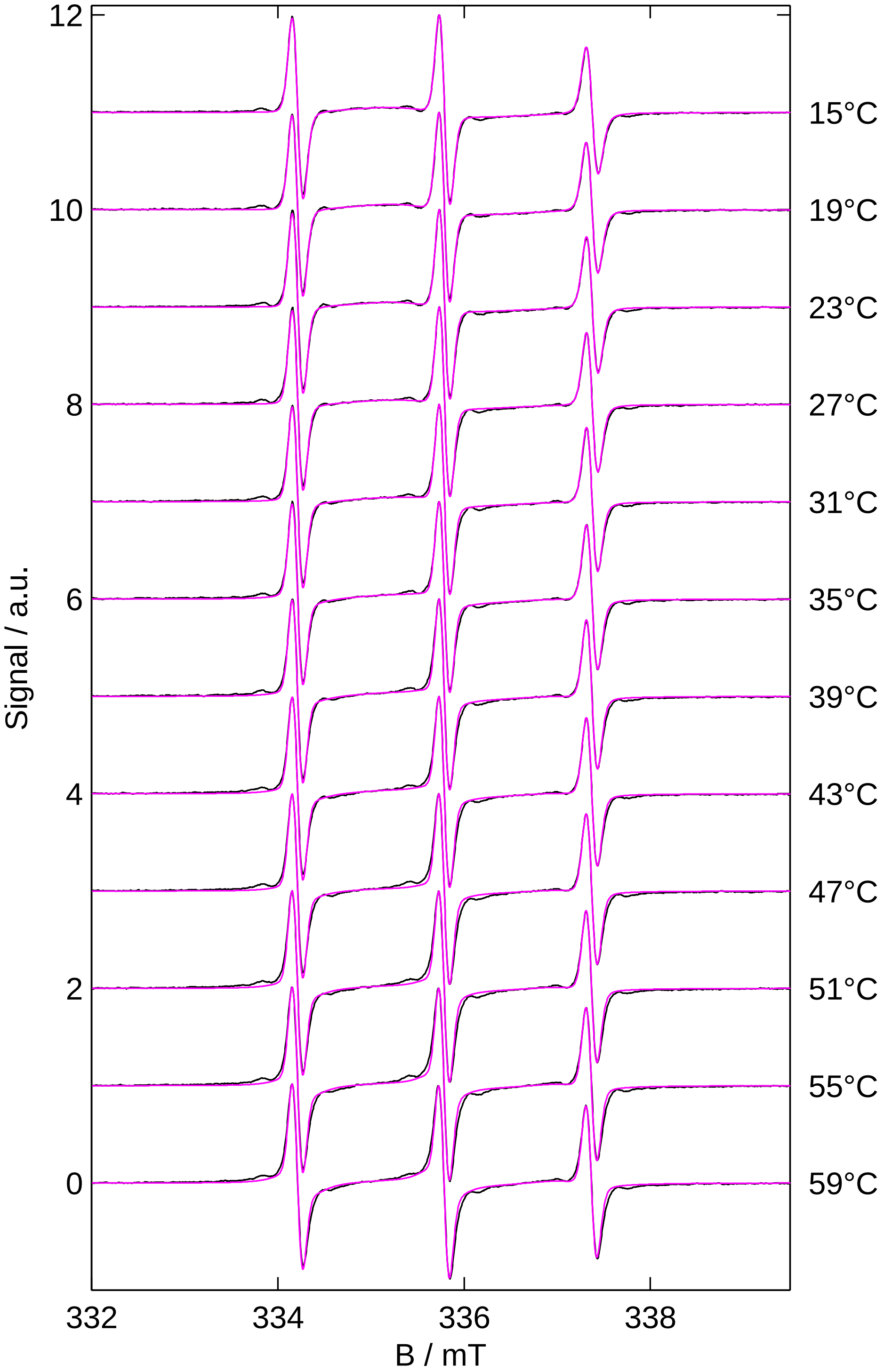

Figure SI 15: All EPR spectral simulations of ELP 200-60 (100 µM) with 16-DSA (600 µM) at temperatures between 15 and 59 °C. Experimental data is shown in black, simulated data in magenta.

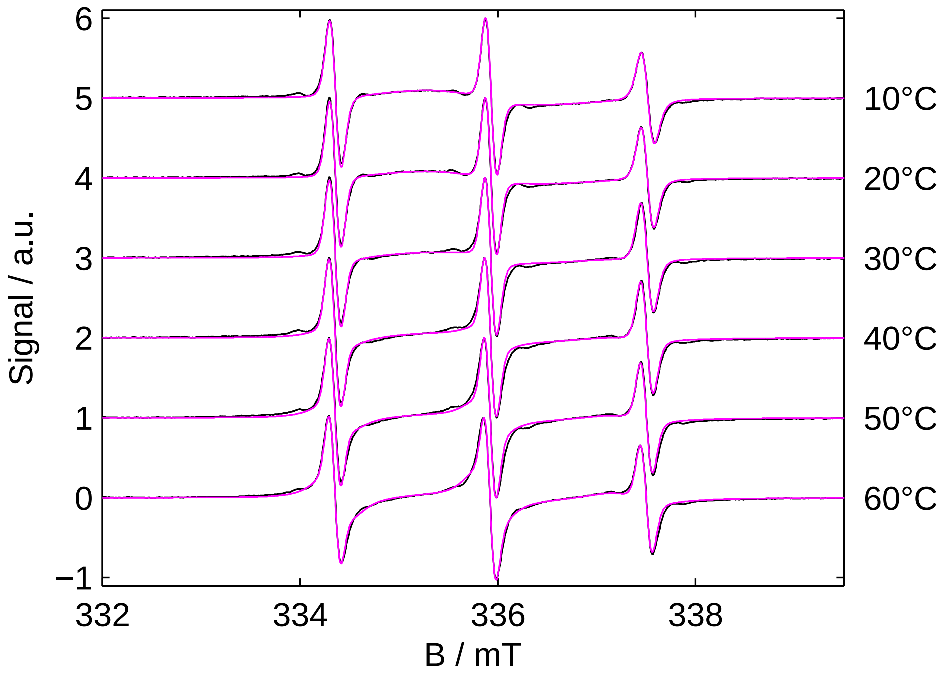

Figure SI 16: All EPR spectral simulations of ELP 200-60 (300 µM) with 16-DSA (600 µM) at temperatures between 10 and 60 °C. Experimental data is shown in black, simulated data in magenta.

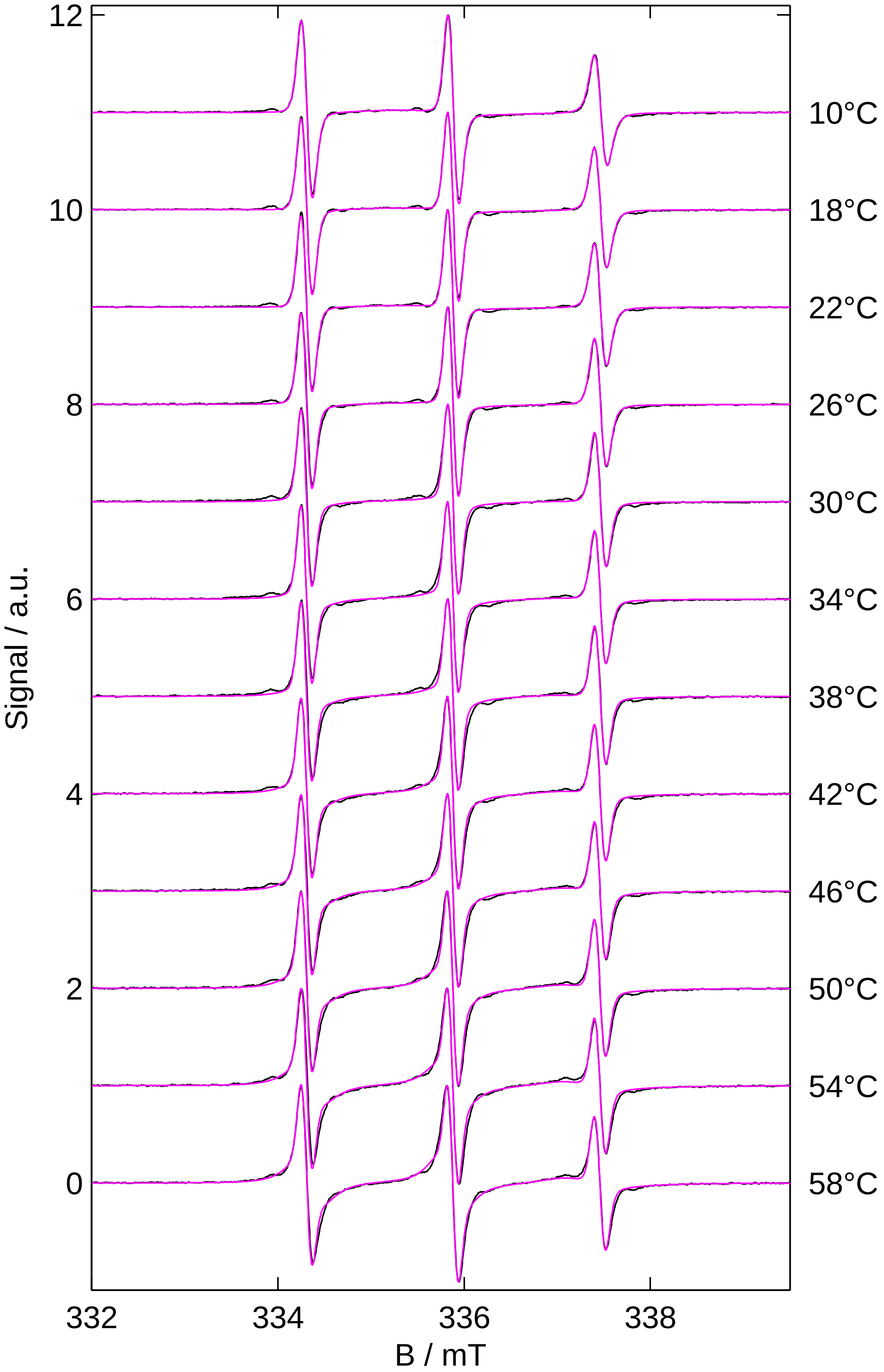

Figure SI 17: All EPR spectral simulations of ELP 200-60 (300 µM) with 16-DSA (400 µM) at temperatures between 10 and 58 °C. Experimental data is shown in black, simulated data in magenta.

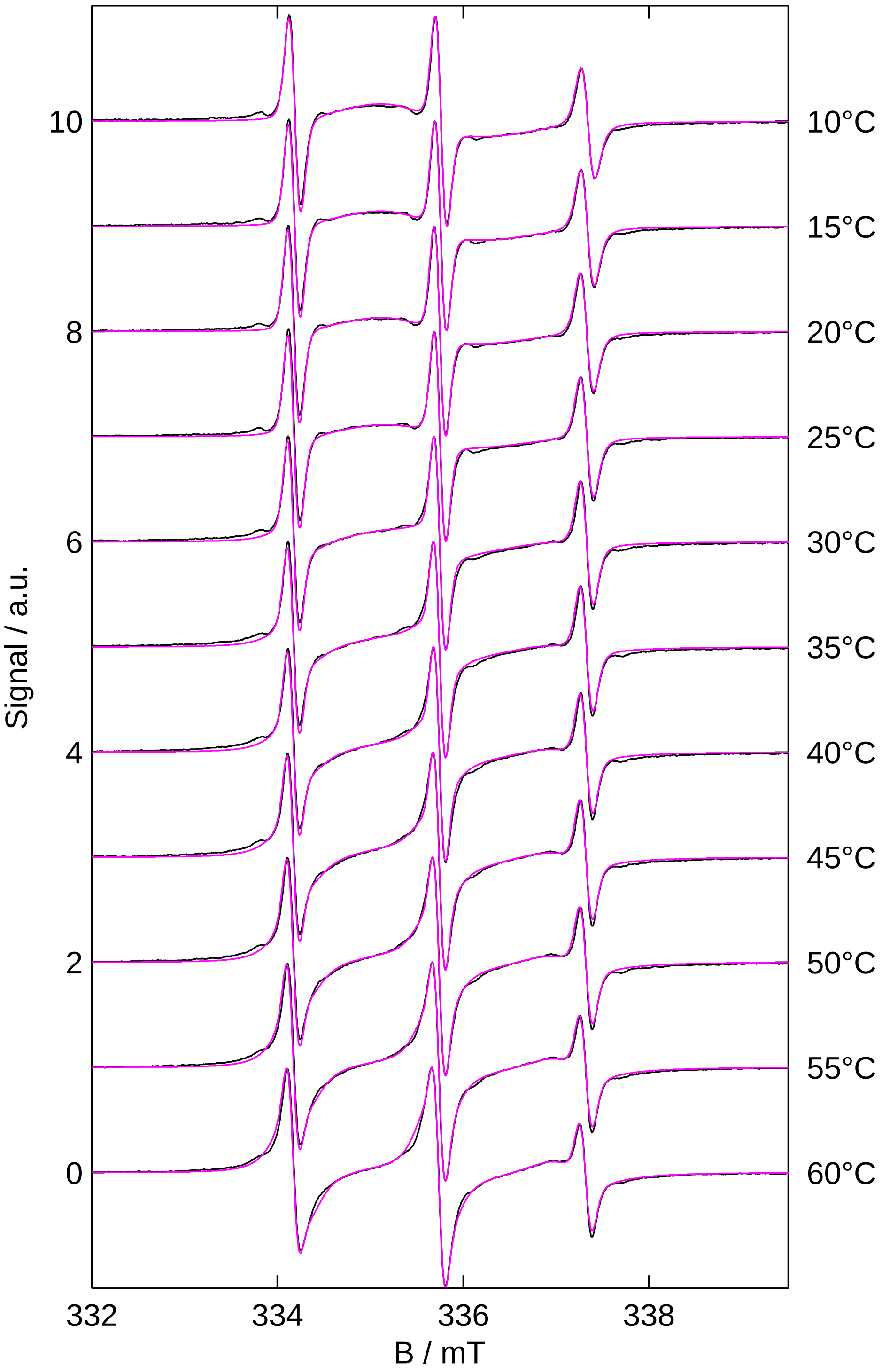

Figure SI 18: All EPR spectral simulations of ELP 200-60 (500 µM) with 16-DSA (1 mM) at temperatures between 10 and 60 °C. Experimental data is shown in black, simulated data in magenta.

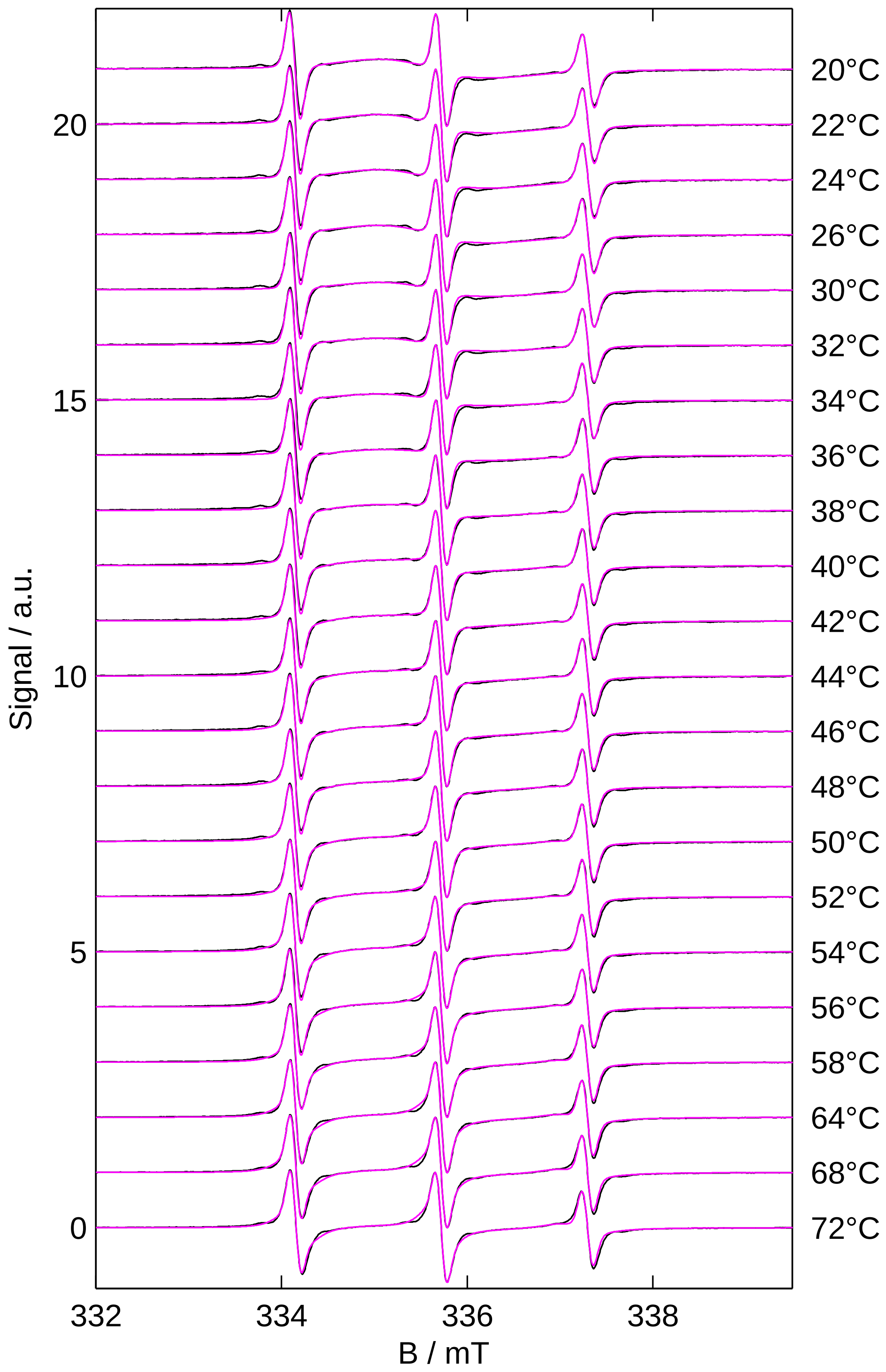

Figure SI 19: All EPR spectral simulations of ELP 40-60 (500 µM) with 16-DSA (1 mM) at temperatures between 20 and 72 °C. Experimental data is shown in black, simulated data in magenta.

5 Simulation results

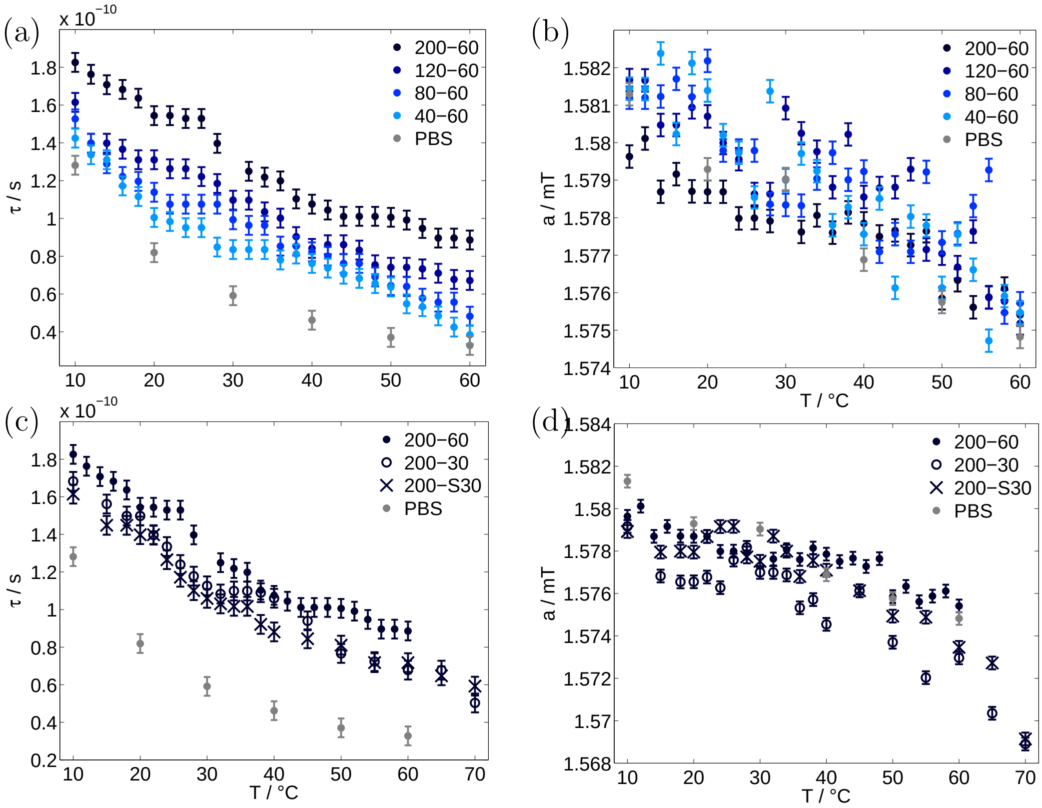

Figure SI 20: Results of simulation: rotational correlation times ((a) and (c)) and hyperfine splitting constant ((b) and (d)) of the hydrophilic spectral component for different hydrophobic block lengths ((a) and (b)) and different hydrophilic blocks ((c) and (d))

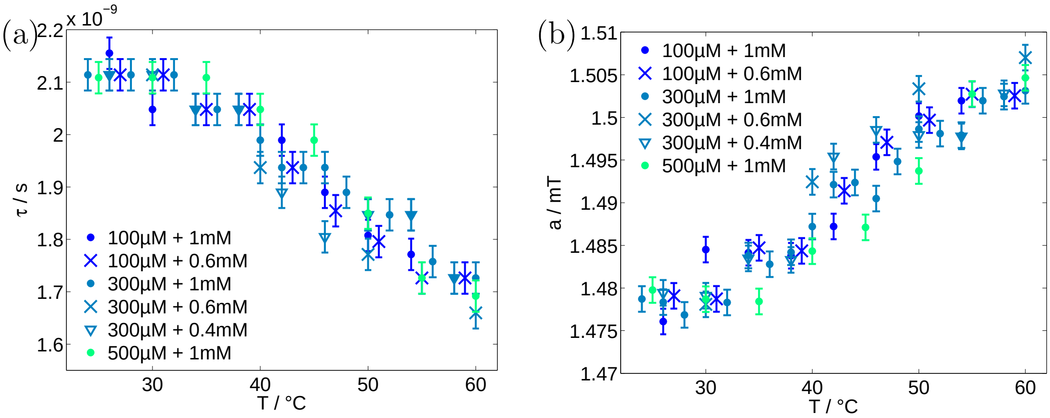

Figure SI 21: Results of simulation of diblock ELP 200-60 (various concentrations) with 16-DSA (various concentrations): rotational correlation times (a) and hyperfine splitting constant (b) of the hydrophobic spectral component

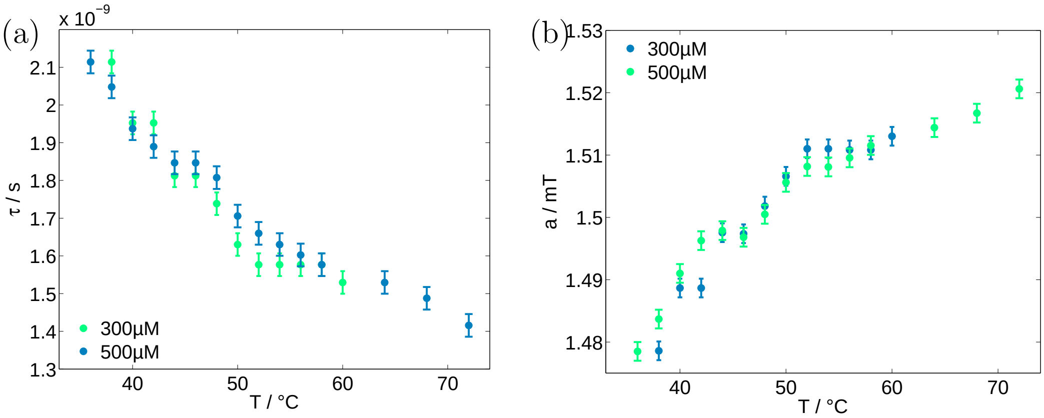

Figure SI 22: Results of simulation of diblock ELP 40-60 (various concentrations) with 16-DSA (various concentrations): rotational correlation times (a) and hyperfine splitting constant (b) of the hydrophobic spectral component

Since the concentration of polymer as well as of spin probe has no significant effect on the rotational correlation time and the hyperfine splitting constant, it can be ruled out that the higher hydrophobicity sensed by the probe is a result of a diminished contact area between hydrophobic and hydrophilic regions for higher x_1.

References

1 E. Garanger, S. R. MacEwan, O. Sandre, A. Brûlet, L. Bataille, A. Chilkoti and S. Lecommandoux, *Macromolecules*, 2015, **48**, 6617–6627.

2 S. Stoll and A. Schweiger, *Journal of Magnetic Resonance*, 2006, **178**, 42–55.

3 M. Ge, S. B. Rananavare and J. H. Freed, *Biochimica et Biophysica Acta*, 1990, **1036**, 228–236.

4 Y. Akdogan, J. Heller, H. Zimmermann and D. Hinderberger, *Physical Chemistry Chemical Physics*, 2010, **12**, 7874–7882.

5 K. Moebius, A. Savitsky, C. Wegener, M. Plato, M. Fuchs, A. Schnegg, A. A. Dubinskii, Y. A. Grishin, I. A. Grigor'ev, M. Kuehn, D. Duché, H. Zimmermann and H.-J. Steinhoff, *Magn. Reson. Chem.*, 2005, **43**, S4–S19.